Dynamic Scaling, Island Size Distribution, and Morphology in the Aggregation Regime of Submonolayer Pentacene Films

Ricardo Ruiz,[1,*] Bert Nickel,[2,3,†] Norbert Koch,[3,4] Leonard C. Feldman,[1] Richard F. Haglund, Jr.,[1] Antoine Kahn,[3,4] Fereydoon Family,[5] and Giacinto Scoles[2,3]

[1]*Vanderbilt University, Department of Physics and Astronomy, Nashville, Tennessee 37235, USA*
[2]*Princeton University, Chemistry Department, Princeton, New Jersey, 08544, USA*
[3]*Princeton Materials Institute, Princeton, New Jersey 08544, USA*
[4]*Princeton University, Department of Electrical Engineering, Princeton, New Jersey 08544, USA*
[5]*Emory University, Department of Physics, Atlanta, Georgia 30322, USA*

(Received 25 June 2003; published 23 September 2003)

Scaling behavior of the island size distribution through a universal scaling function $f(u)$ is demonstrated for submonolayer pentacene islands in the aggregation regime ($0.1 < \theta < 0.5$) grown on oxidized silicon surfaces. The distribution of $f(u)$ suggests that four molecules constitute the smallest stable island. The structure factor $S(\mathbf{k})$ of the submonolayer films calculated from AFM micrographs compares well with diffuse x-ray intensities from *in situ* experiments. The structure factor was decomposed into the contribution from the average island shape and the interisland distribution confirming that a unique characteristic length scale regulates the growth dynamics.

DOI: 10.1103/PhysRevLett.91.136102 PACS numbers: 68.43.Jk, 61.10.Eq, 68.37.Ps, 68.55.Ac

Testing physics models for the growth of organic thin films prepared by organic molecular beam deposition (OMBD) is a topic of substantial interest in thin-film science [1–4]. In inorganic thin-film growth by molecular beam epitaxy (MBE), the diffusion-limited aggregation (DLA) model [5–7] led to predictions of the fractal character of individual aggregates and has also been employed to formulate scaling theories to describe the island size distribution and its evolution with coverage during MBE film formation. However, little analogous quantitative information exists about the applicability of diffusion models to organic films prepared by OMBD.

Efforts have been made to adapt scaling theories to three-dimensional (3D) aggregates grown by OMBD [3,8,9] and to 2D systems prepared from solution [10,11]. Use of diffusion concepts to OMBD include the surface diffusion of single molecules [12] and the fractal shape of pentacene aggregates [4]. However, a diffusion model has not yet been fully tested on 2D OMBD films. In this Letter, we demonstrate the applicability of a dynamic scaling model to the 2D diffusion-mediated growth of pentacene ($C_{22}H_{14}$) on silicon oxide, an organic/inorganic interface widely used for transistor applications [13].

Diffusion mediated growth involves four qualitatively different steps [14,15]. Initially, monomers diffuse on an almost bare substrate and, when a critical number of them meet, a stable nucleus is formed. In a second (intermediate) step, adsorbates still nucleate new islands but also start aggregating into existing ones. Then, in the aggregation regime, the incoming material aggregates into the existing islands only. Finally islands coalesce.

The kinetics of the diffusion process, characterized by the ratio of the diffusion constant D to the incoming flux F ($R = D/F$), determines system-specific properties such as the nucleation density, N, the average island size, $A(\theta)$, and the interisland separation, ξ_m, through

$$N = CR^{-\chi} \simeq \xi_m^{-2} \simeq \theta/A(\theta), \tag{1}$$

where θ is the coverage, C is a proportionality constant, and the exponent χ is related to the critical island size, i, by $\chi = i/(i+2)$ [15–17]. The value of i is expressed in number of monomers. Islands larger than i are stable against dissociation.

The aggregation regime ($0.1 < \theta < 0.5$) is of particular interest because it shows a scaling behavior of the island size distribution and presents only one characteristic interisland length scale [14] which, together with the fractal dimension of the islands, constitutes a fingerprint of diffusion-mediated growth.

According to the dynamic scaling assumption [14,18–20], the distribution of islands of size a per unit area, $N_a(\theta)$, scales with the average island size $A(\theta) = [\sum aN_a(\theta)]/\sum N_a(\theta)$ as

$$N_a(\theta) = \theta A(\theta)^{-2} f(u). \tag{2}$$

Here, $u = a/A(\theta)$ and $f(u)$ is a dimensionless θ-independent scaling function that contains all system-specific information. The particular distribution of the scaling function is determined by the critical island size i. Based on numerical simulations, an empirical expression for the scaling function has been constructed [21]:

$$f(u) = C_i u^i \exp(-b_i i u^{1/b_i}), \tag{3}$$

where C_i and b_i are fixed by implicit geometrical equations [22] which assure normalization and proper asymptotic behavior of $f(u)$.

In these experiments, pentacene films were evaporated in (ultra)high vacuum onto chemically oxidized Si

substrates kept at room temperature (RT) with a deposition rate of ~0.75 Å/min. Details on the sample preparation can be found elsewhere [23]. Characterization was carried out by *ex situ* tapping mode atomic force microscopy (AFM) and *in situ* x-ray scattering at the National Synchrotron Light Source.

The inset of Fig. 1 shows two examples of pentacene films at coverages of $\theta = 0.18$ and 0.42 ML. The island size distributions, $N_a(\theta)$, can be measured from an AFM micrograph and are plotted for different coverages in Fig. 1(a), where a is expressed in μm^2 and N_a in μm^{-4} as a distribution density such that $\int N_a da = N$. For each coverage, $N_a(\theta)$ exhibits a well-defined maximum at $A(\theta)$. The average island size increases with increasing θ and the distribution broadens. After rescaling according to Eq. (2), all data collapse into a single scaling function $f(u)$, as shown in Fig. 1(b). A least squares fit of the data with Eq. (3) gives $i = 3$ [solid line in Fig. 1(b)] as the best fit to the critical cluster size, suggesting that the smallest stable cluster is composed of four molecules [inset of Fig. 1(b)]. As a comparison, $f_i(u)$ for $i = 1$ is also plotted (dashed line) showing that the existence of stable dimers

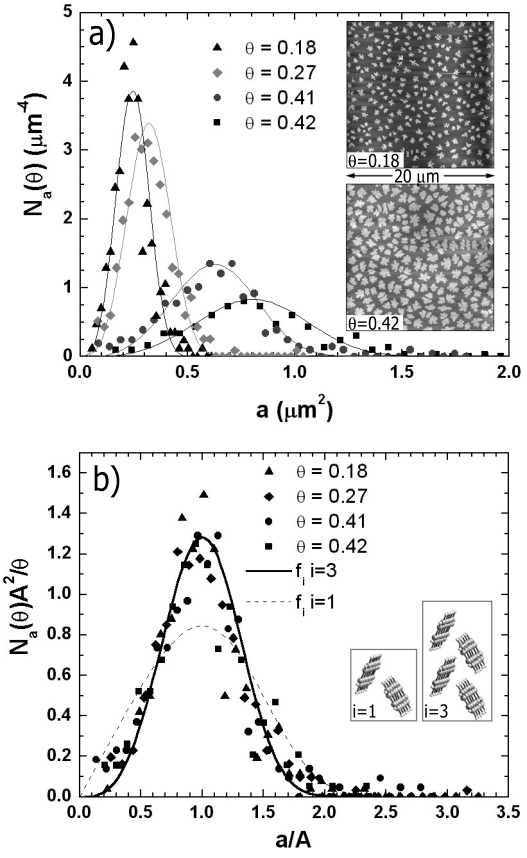

FIG. 1. (a) Island size distribution $N_a(\theta)$ of pentacene islands at various coverages. Inset: AFM micrographs of pentacene islands at 0.18 and 0.42 ML (b) Scaled island size distribution. The scaling function $f(u)$ for a critical cluster size of ($i = 3$) is indicated by the solid curve [See Eq. (3)].

can be ruled out. The quantitative agreement of the scaling function with the data indicates that pentacene on silicon oxide exhibits DLA growth behavior. The Hausdorff (fractal) dimension of 20 islands at $\theta = 0.18$ was also measured applying a box-counting method [24], obtaining an average value of $d_f = 1.83 \pm 0.01$, close to the DLA value of $d_f \approx 1.7$ [5,24,25].

More information on the growth dynamics and island correlations is contained in the structure factor $S(\mathbf{k}) \sim |FT[\tilde{n}(\mathbf{r})]|^2$, where FT denotes a Fourier transformation and $\tilde{n}(\mathbf{r}) = n(\mathbf{r}) - \theta$ is the mass density $n(\mathbf{r})$, offset by the coverage so that $S(\mathbf{0}) = 0$. Experimentally, $n(\mathbf{r})$ can be obtained from an AFM micrograph [$n(\mathbf{r}) = 1$, where there is pentacene and $n(\mathbf{r}) = 0$ otherwise]. $S(\mathbf{k})$ is then obtained from the power spectral density (PSD) of $\tilde{n}(\mathbf{r})$.

A characteristic island separation ξ_m originates a maximum of intensity in the circularly averaged structure factor $S(|\mathbf{k}|)$ at $|\mathbf{k}| = k_m$, with $k_m = 2\pi/\xi_m$. The amplitude of this maximum also shows scale invariance [14].

The ringlike structure factor $S(\mathbf{k})$ of pentacene films is shown as the inset of Fig. 2 for a coverage $\theta = 0.18$. Circularly averaged structure factors $S(k)$ extracted from these 2D maps are shown in Fig. 2(a). The maxima of $S(k)$ occurring at $k_m \approx 4.1\ \mu\text{m}^{-1}$ are indicated accordingly. The values of k_m and $A(\theta)$ can be used to verify the scaling assumption [Eq. (1)]. Table I shows that there is reasonable agreement between N, $A(\theta)$, and k_m throughout the aggregation regime. The scaling of $S(k_m)$ with coverage is verified in Fig. 2(b), although $S(k_m)$ scaled with θ^{-1} instead of the $(\theta - \theta^2)^{-1}$ predicted by the model [14]. The reason for this is still unclear.

Assuming that the submonolayer film $\tilde{n}(\mathbf{r})$ is made of identical islands $n_1(\mathbf{r})$, then $\tilde{n}(\mathbf{r})$ may be obtained by convolving $n_1(\mathbf{r})$ with an array of delta functions $n_2(\mathbf{r})$ located at the island centers of mass: $\tilde{n}(\mathbf{r}) = n_1(\mathbf{r}) \otimes n_2(\mathbf{r})$. The convolution theorem implies that the structure factor $S(k)$ can be decomposed into the product of the single island form factor $F_1(k) = |FT[n_1(\mathbf{r})]|^2$, and the structure factor of the island distribution $F_2(k) = |FT[n_2(\mathbf{r})]|^2$. Thus, the total structure factor $S(\mathbf{k})$ is given by [14]

$$S(\mathbf{k}) \sim F_1(k)F_2(k). \tag{4}$$

For small k ($k < k_D = 2\pi/\xi_D$), a plateau is expected in $F_1(k)$ [26] with ξ_D denoting the island average lateral size while, for $k \gg k_D$, $F_1(k)$ exhibits an asymptotic power law decay. For $F_2(k)$, less detailed predictions exist, but at least a sharp rise is expected at $F_2(k = k_m)$, corresponding to the island-island correlation distance. For $k \gg k_m$, F_2 is expected to remain nearly constant assuming that the interisland contributions to $S(k)$ are constant for large k.

This is shown for pentacene films at a coverage of 0.18 ML in Fig. 2(c). The island form factor $F_1(k)$ [thick

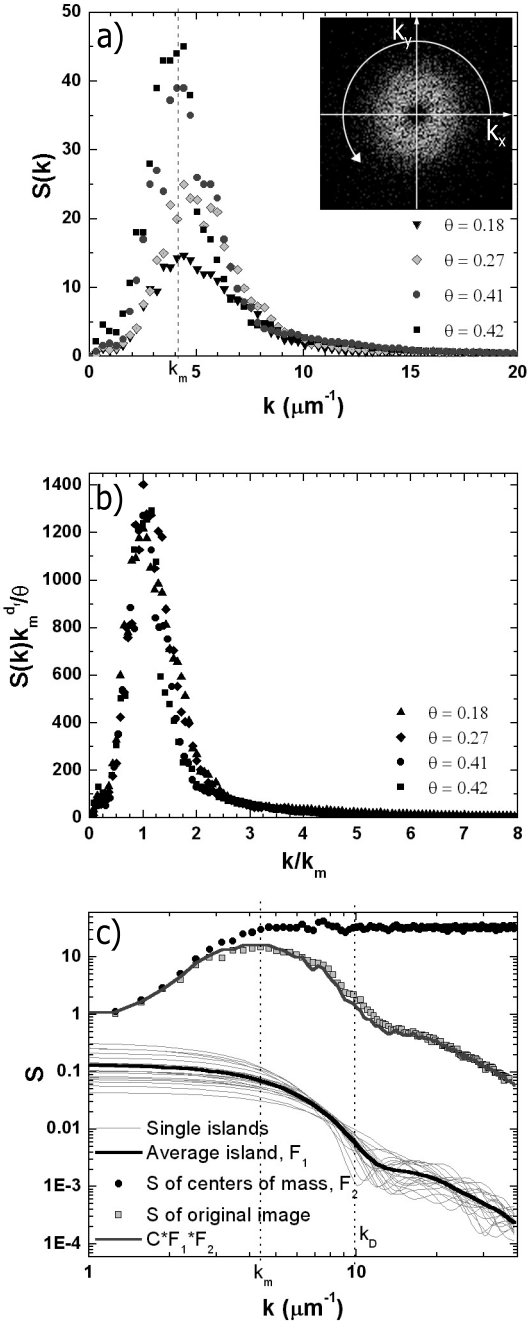

FIG. 2. $S(k)$ as obtained from AFM data. (a) Circularly averaged structure factor $S(k)$ for pentacene islands at various coverages. Inset: power density spectrum $S(\mathbf{k})$ for $\theta = 0.18$. (b) Scaled structure factor. (c) Structure factor decomposition for $\theta = 0.18$. The structure factor $S(k)$ (solid squares), the single-island form factor $F_1(k)$ (thick solid line), and the structure factor of the island distribution $F_2(k)$ (dots), as determined from an AFM micrograph. The product of $F_1(k)$ and $F_2(k)$ is shown as a gray line; k_m and k_D are marked with vertical dotted lines.

solid line in Fig. 2(c)] is obtained from the average over 20 isolated islands [thin solid lines in Fig. 2(c)]. The form factor of each of the 20 individual islands was obtained by isolating the islands from a binary AFM micrograph and then computing their PSD separately. $F_1(k)$ shows the expected (small angle scattering similar to [26]) functional form, i.e., an extended plateau up to $2\pi/\xi_D$ and a power law behavior for $k > k_D$. In turn, F_2 [dots in Fig. 2(c)] is obtained by calculating the PSD of an assembly of area-weighted delta functions located at the centers of mass of the individual islands of the AFM image. F_2 exhibits a very smooth, error-function-like behavior, with a constant level above k_m and a fast decrease below. This step produces the maximum in the structure factor $S(k)$ [solid squares in Fig. 2(c)]. The calculated functions $F_1(k)$ and $F_2(k)$ may be used to check the validity of Eq. (4). Indeed, the product of $F_1(k)$ and $F_2(k)$ [gray solid line in Fig. 2(c)] matches well with the structure factor $S(k)$ [solid squares in Fig. 2(c)].

TABLE I. Nucleation densities and characteristic length scales. N, $\theta/A(\theta)$, and ξ_m^{-2} are expressed in (μm^{-2}).

θ	N	$\theta/A(\theta)$	$\xi_m^{-2} = [k_m/(2\pi)]^2$
0.18	0.7	0.7	0.5
0.27	0.8	0.8	0.5
0.41	0.6	0.6	0.4
0.42	0.5	0.5	0.4

At high k ($k > k_m$), $F_2 \sim$ const and the structure factor $S(k)$ is dominated by the power law decay of F_1. Using $d_f = 1.83$ and assuming a fractal object, we obtained $k_D = 9.9$ as shown in Fig. 2(c), confirming that the plateau of the island form factor extends for $k < k_D$.

Since $\tilde{n}(\mathbf{r})$ gives rise to diffuse scattering, the structure factor may also be accessed over large areas by synchrotron x-ray scattering [27]. In the kinematical approximation [28], $I_D(\mathbf{k}) \sim S(\mathbf{k})$, where I_D is the diffuse scattered intensity. $I_D(\mathbf{k})$ close to the specular condition was measured on samples grown at RT ($\sim 295 \pm 3$ K)and at 273 K by varying the x-ray angle of incidence (''rocking scan''). The diffuse intensities are depicted in Fig. 3. Additional specular intensity at $k_{||} = 0$ gives rise to a (resolution limited) δ-shaped contribution. Furthermore, the peaking of the transmission function gives rise to Yoneda scattering at the critical angles (here: $|k_{||}| \simeq 0.0038$ Å^{-1}). With increasing coverage, the diffuse intensity increases and two symmetric satellites at $|k_{||}| = k_m$ are observed. Because of the diffraction geometry and the narrow shape of the detector slits, the x-ray experiments provide sharp resolution only in one direction. Intensities along the other direction are integrated [27] and therefore the maximum is less pronounced. The RT value of $k_m = 5.6$ μm^{-1} agrees with the AFM measurements within $\sim$20%, which is in excellent agreement given that the RT samples were not temperature controlled. The diffuse x-ray scattering intensities also scale with the coverage as $I(k, \theta) \sim \theta$ in good agreement with the behavior of the structure factor $S(k)$ of the samples used for the AFM

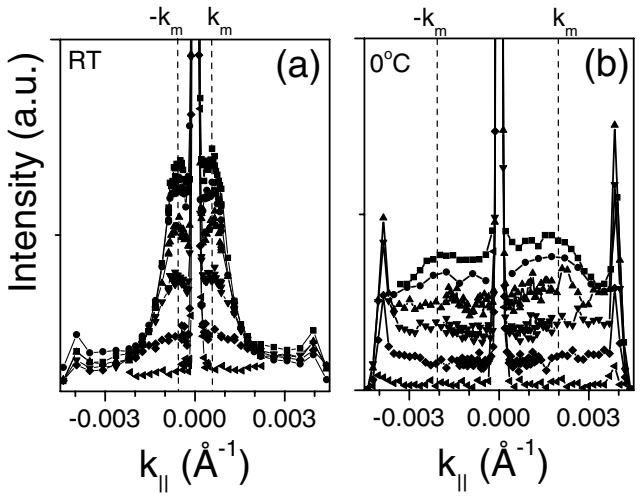

FIG. 3. X-ray measurements. (a) Growth at RT, coverages are $\theta = (0, 0.1, 0.2, 0.3, 0.4, 0.54)$. (b) Growth at 0 °C, coverages are $\theta = (0, 0.1, 0.2, 0.3, 0.4, 0.5)$.

analysis. For the sample grown at 273 K [Fig. 3(b)], the surface diffusivity of the molecules was significantly reduced yielding a larger nucleation density and a smaller interisland distance as indicated by a ~4 times larger k_m, thus reflecting the thermally activated nature of the diffusion constant D.

In summary, these AFM and x-ray studies confirm the diffusion-mediated scaling behavior of the island size distribution and yield a critical island size of four molecules. The structure factor $S(\mathbf{k})$ of the submonolayer films was calculated from AFM micrographs and compares well with diffuse x-ray intensities obtained by *in situ* synchrotron experiments. The decomposition into the contribution from the island form factor, F_1, and the structure factor of the island distribution, F_2, confirms a characteristic length scale ξ_m governing the island separation and the average island size $A(\theta)$, thus confirming dynamic scaling for pentacene submonolayer growth. Finally, a strong temperature dependence of the characteristic length scale was observed. We have shown that the growth of pentacene on oxidized Si at room temperature is diffusion mediated and that existing scaling theories can be fully applied to this organic/inorganic system.

We thank the NSLS management, beamline staff, and scientists from Exxon for continuous support. The work at Princeton and at NSLS has been supported by the DOE under Grant No. DE-FG02-93ER45503. R. R. acknowledges the support of a Vanderbilt University Discovery Grant. The authors thank J. G. Amar, P.-M. Lam, and R. López for valuable discussions.

*Current address: Cornell University, Cornell Center for Materials Research, Ithaca, NY 14853, USA.

†Author to whom correspondence may be addressed. Current address: Ludwig-Maximilians-Universität, 80539 München, Germany. Electronic address: Bert.Nickel@physik.uni-muenchen.de

[1] F. Biscarini, R. Zamboni, P. Samon, P. Ostoja, and C. Taliani, Phys. Rev. B **52**, 14 868 (1995).
[2] S. Forrest and Y. Zhang, Phys. Rev. B **49**, 11297 (1994).
[3] M. Brinkmann, F. Biscarini, C. Taliani, I. Aiello, and M. Ghedini, Phys. Rev. B **61**, R16 339 (2000).
[4] Frank-J. Meyer Zu Heringdorf, M. C. Reuter, and R. M. Tromp, Nature (London) **412**, 517 (2001).
[5] T. A. Witten, Jr. and L. M. Sander, Phys. Rev. Lett. **47**, 1400 (1981).
[6] P. Meakin, Phys. Rev. Lett. **51**, 1119 (1983).
[7] M. Kolb, R. Botet, and R. Jullien, Phys. Rev. Lett. **51**, 1123 (1983).
[8] F. Biscarini, P. Samori, O. Greco, and R. Zamboni, Phys. Rev. Lett. **78**, 2389 (1997).
[9] M. Brinkmann, S. Graff, and F. Biscarini, Phys. Rev. B **66**, 165430 (2002).
[10] I. Doudevski, W. A. Hayes, and D. K. Schwartz, Phys. Rev. Lett. **81**, 4927 (1998).
[11] I. Doudevski and D. K. Schwartz, Phys. Rev. B **60**, 14 (1999).
[12] M. Schunack, T. R. Linderoth, F. Rosei, E. Laegsgaard, I. Stensgaard, and F. Besenbacher, Phys. Rev. Lett. **88**, 156102 (2002).
[13] C. D. Dimitrakopoulos and P. R. L. Malenfant, Adv. Mater. **14**, 99 (2002).
[14] J. G. Amar, F. Family, and P.-M. Lam, Phys. Rev. B **50**, 8781 (1994).
[15] J. A. Venables, G. D. T. Spiller, and M. Hanbücken, Rep. Prog. Phys. **47**, 399 (1984).
[16] J. Evans and M. Bartelt, J. Vac. Sci. Technol. A **12**, 1800 (1994).
[17] J. Stroscio and D. Pierce, Phys. Rev. B **49**, 8522 (1994).
[18] T. Vicsek and F. Family, Phys. Rev. Lett. **52**, 1669 (1984).
[19] F. Family and P. Meakin, Phys. Rev. Lett. **61**, 428 (1988).
[20] M. Zinke-Allmang, L. C. Feldman, and M. H. Grabow, Surf. Sci. Rep. **16**, 377 (1992).
[21] J. G. Amar and F. Family, Phys. Rev. Lett. **74**, 2066 (1995).
[22] The numerical values of C_i and b_i are fixed by the implicit hypergeometrical equations $\{\Gamma[(i+2)b_i]\}/\{\Gamma[(i+1)b_i]\} = (ib_i)^{b_i}$ and $C_i = [(ib_i)^{(i+1)b_i}]/\{b_i\Gamma[(i+1)b_i]\}$.
[23] R. Ruiz, B. Nickel, N. Koch, L. Feldman, R. Haglund, A. Kahn, and G. Scoles, Phys. Rev. B **67**, 125406 (2003).
[24] T. Vicsek, *Fractal Growth Phenomena* (World Scientific, Singapore, 1989).
[25] P. Meakin, Phys. Rev. A **27**, 1495 (1983).
[26] A. Gunier and G. Fournet, *Small-Angle Scattering of X-rays* (Wiley, New York, 1955).
[27] M. Tolan, O. H. Seeck, J.-P. Schlomka, W. Press, J. Wang, S. K. Sinha, Z. Li, M. H. Rafailovich, and J. Sokolov, Phys. Rev. Lett. **81**, 2731 (1998).
[28] B. E. Warren, *X-Rays Diffraction* (Addison-Wesley, Reading, Massachusetts, 1969).